Advanced diffraction and scattering (ADS 1 & ADS 2) beamline

AOFSRR school 14th Aug 2024

Presented by Dr. Yang Cao; caoy@ansto.gov.au

ADS science team: Dr. Justin Kimpton, Dr. Josie Auckett, Dr. Yang Cao

Australian Government | ANSTO

AS beamlines

	Original beamlines	BRIGHT beamlines
SPECTROSCOPY	SXR, XAS	MEX-1, MEX-2
IMAGING	IMBL	MCT
MICROSCOPY	XFM, THz, IR	Nanoprobe
SCATTERING	SAXS/WAXS	BioSAXS
CRYSTALLOGRAPHY	MX1&2	MX3
DIFFRACTION	PD	ADS1&2

ANSTO

Where do we fit

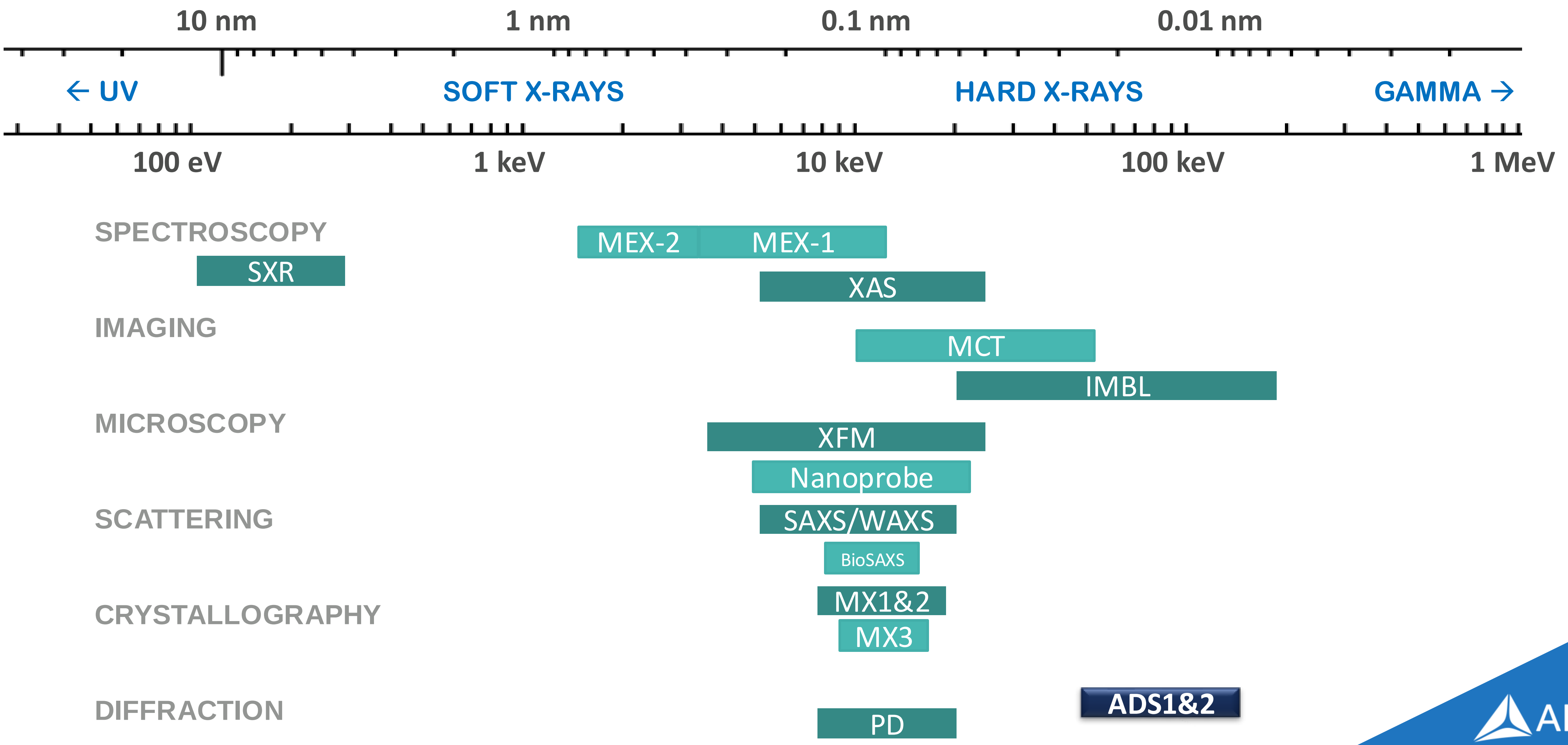

ANSTO

Why high energy ?

- Decreased absorption
  - Increased penetration
  - Less radiation damage to the sample

(Absorption coefficient)

I_0 → μ → I

Beer-Lambert Law: $I = I_0 e^{-\mu t}$

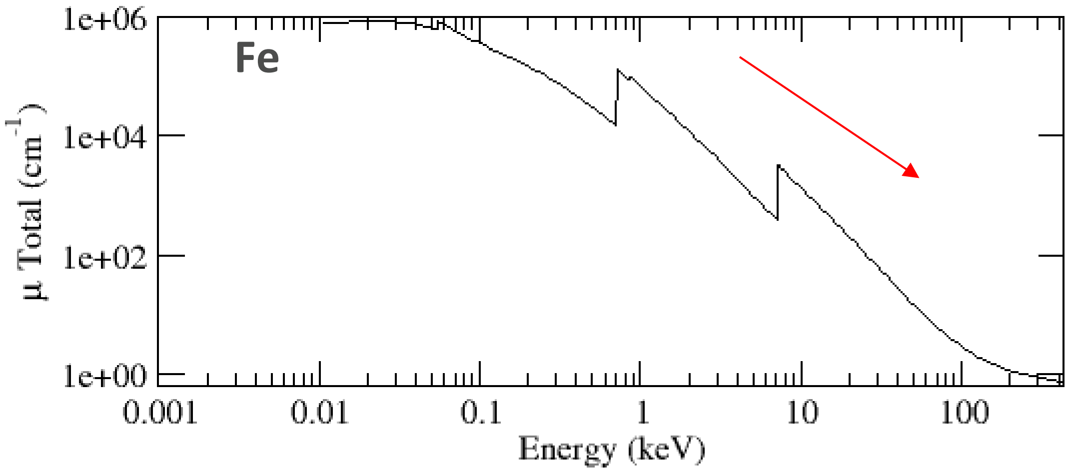

Ideal for sample

✓ with high-Z elements

✓ thick and bulky, e.g., minerals, large metal pieces

✓ in complex sample environments, e.g., reaction cell

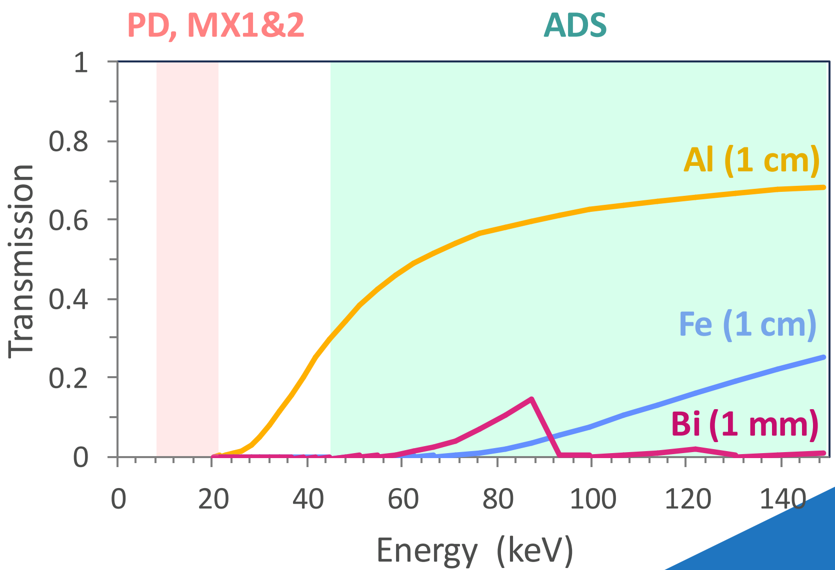

ANSTO

Why high energy ?

- *smaller λ*
  - *n*λ*=2d sinθ*
    - Narrower diffraction angle *θ* - Small beam entrance and exit windows
    - *Smaller d* - Probing shorter length scales within the material
  - *q= 4π sinθ/*λ *(or q = 2π/d)*
    - Accessing high-*q* range – essential for total scattering (PDF analysis)
  - flatten Ewald sphere (radius 1/ λ)
    - Mapping more region on the reciprocal lattice

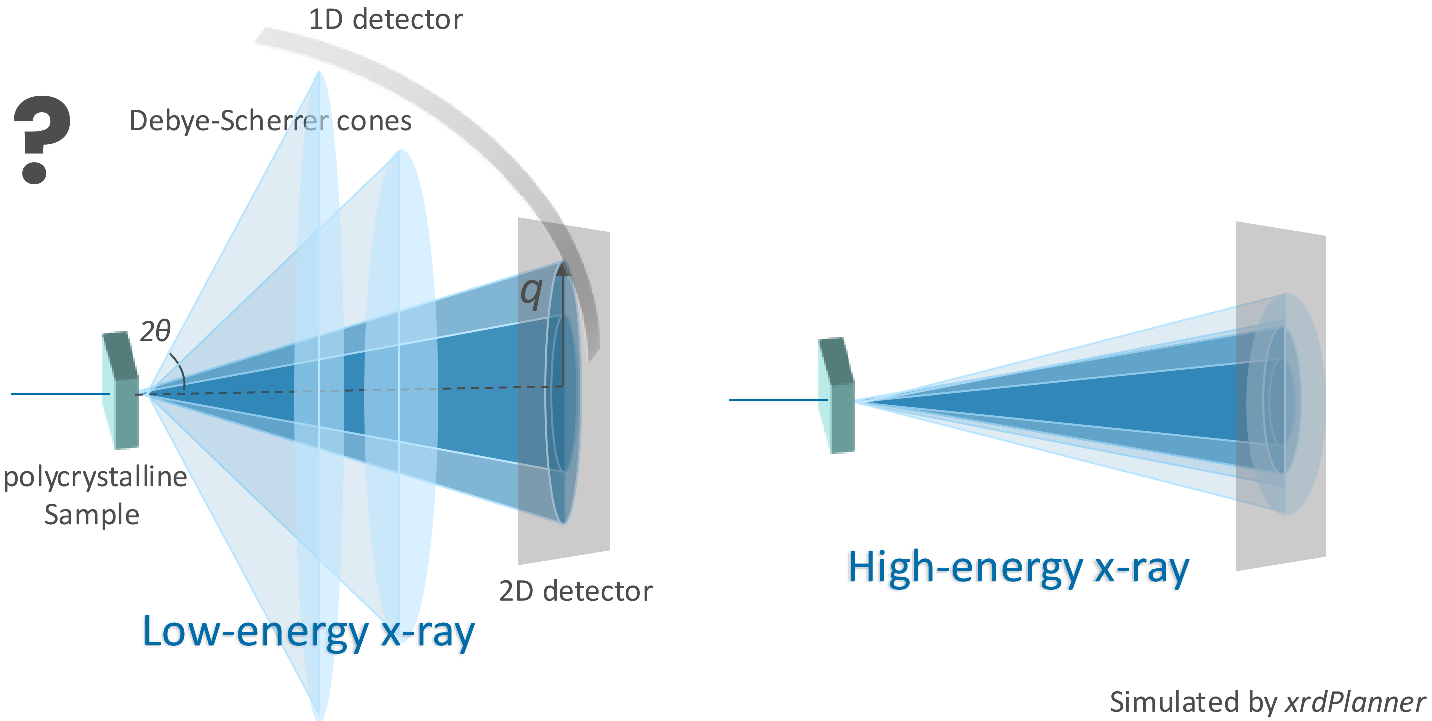

Simulated by *xrdPlanner*

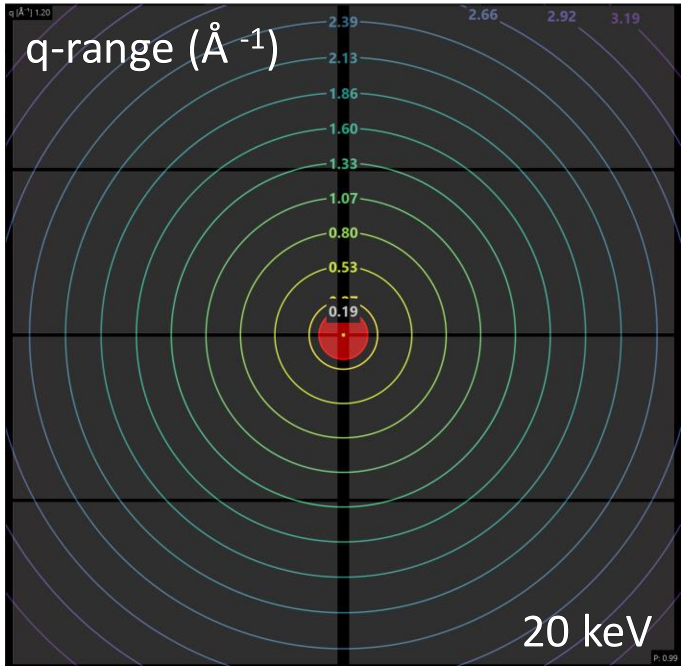

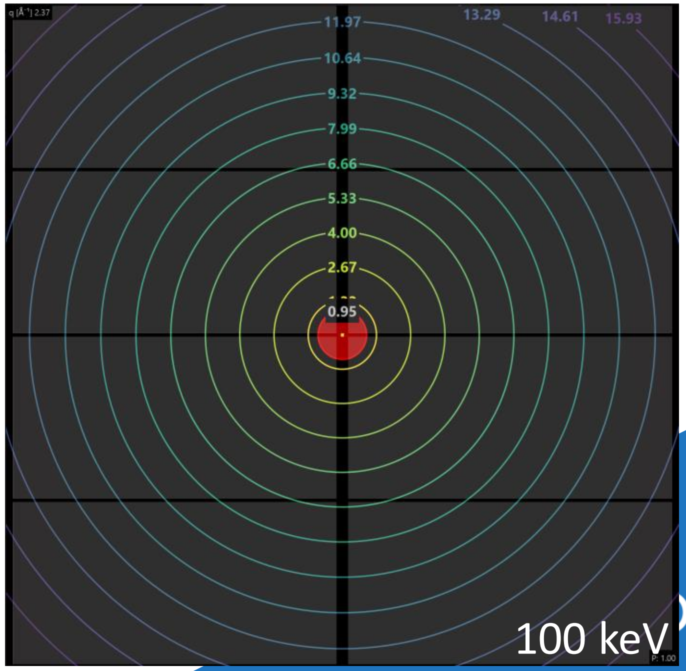

Why high energy ?

- *Smaller λ*
  - $n\lambda = 2d \sin\theta$
    - › Narrower diffraction angle θ - Small beam entrance and exit windows
    - › *Smaller d* - Probing shorter length scales within the material
  - $q = 4\pi \sin\theta/\lambda$ (or $q = 2\pi/d$)
    - › Accessing high-*q* range – essential for total scattering (PDF analysis)
  - flatten Ewald sphere (radius $1/\lambda$)
    - › Mapping more region on the reciprocal lattice

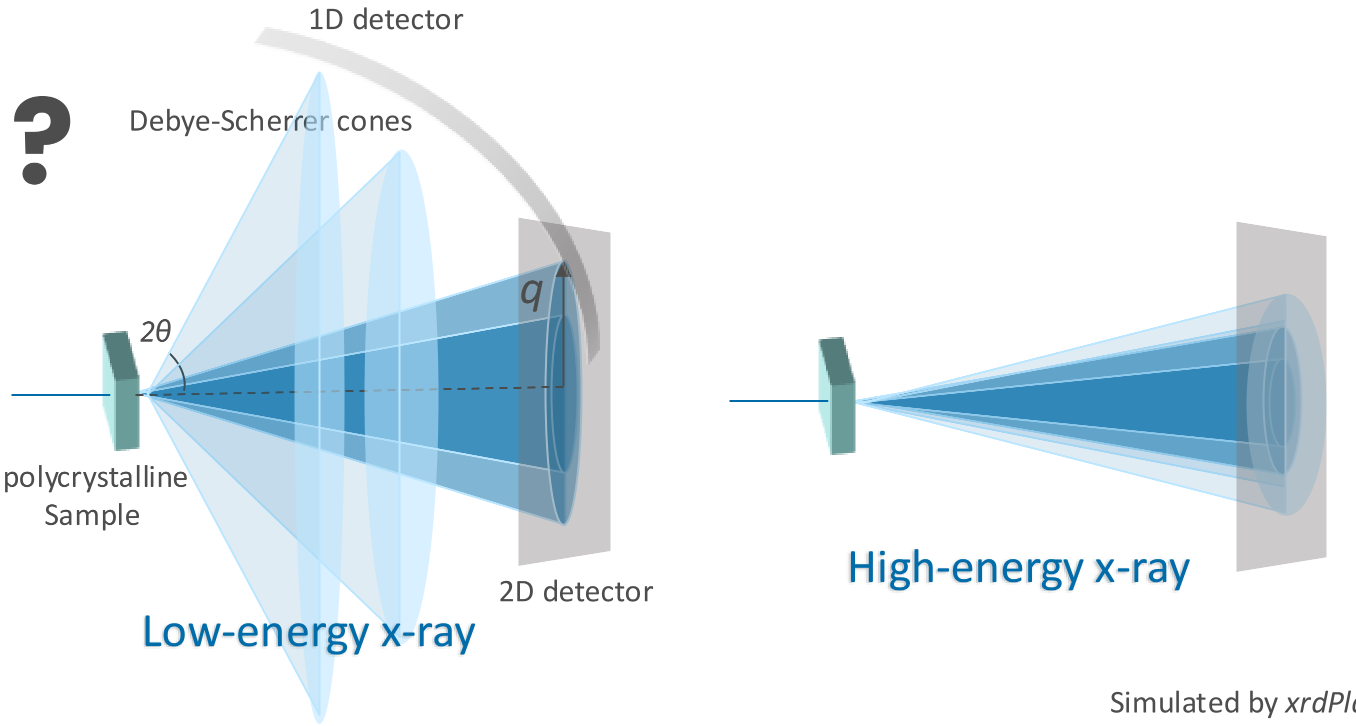

Simulated by *xrdPlanner*

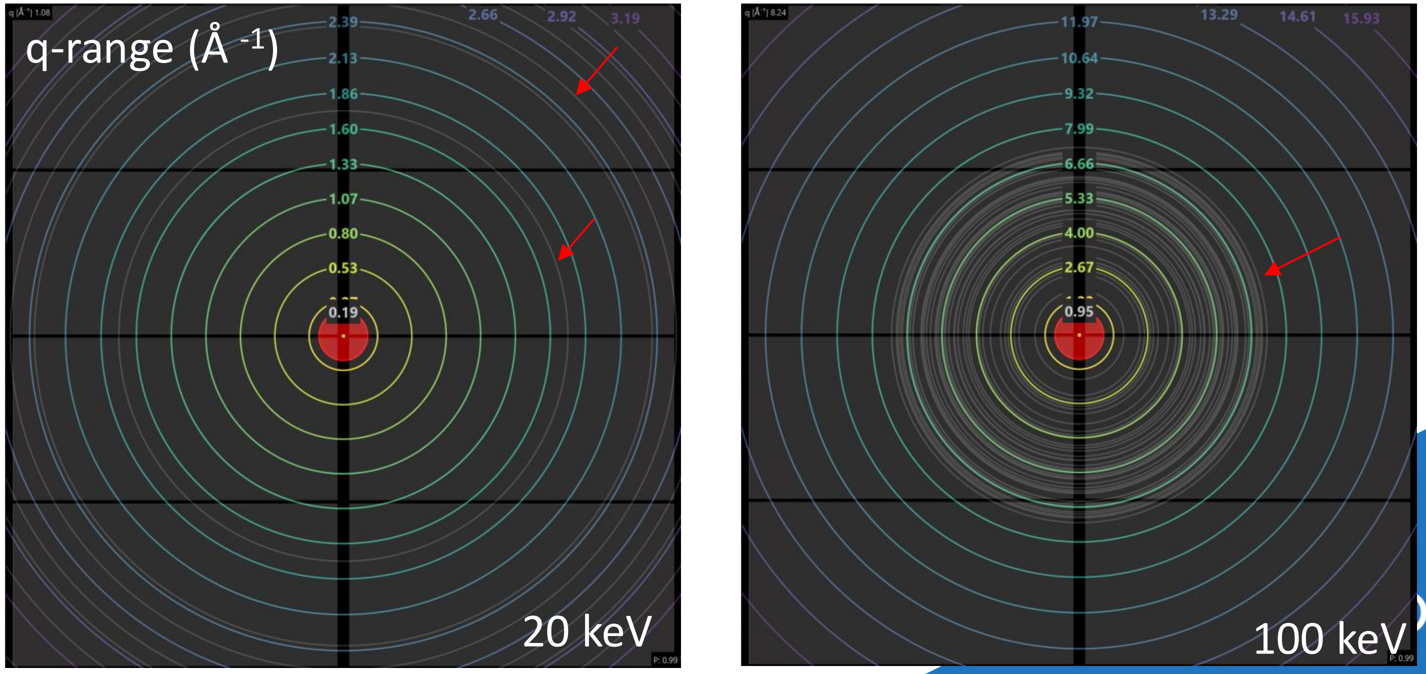

Why high energy ?

- *Smaller λ*
  - *n*λ*=2d sinθ*
    - Narrower diffraction angle *θ* - Small beam entrance and exit windows
    - *Smaller d* - Probing shorter length scales within the material
  - *q= 4π sinθ/*λ *(or q = 2π/d)*
    - Accessing high-*q* range – essential for total scattering (PDF analysis)
  - flatten Ewald sphere (radius 1/ λ)
    - Mapping more region on the reciprocal lattice

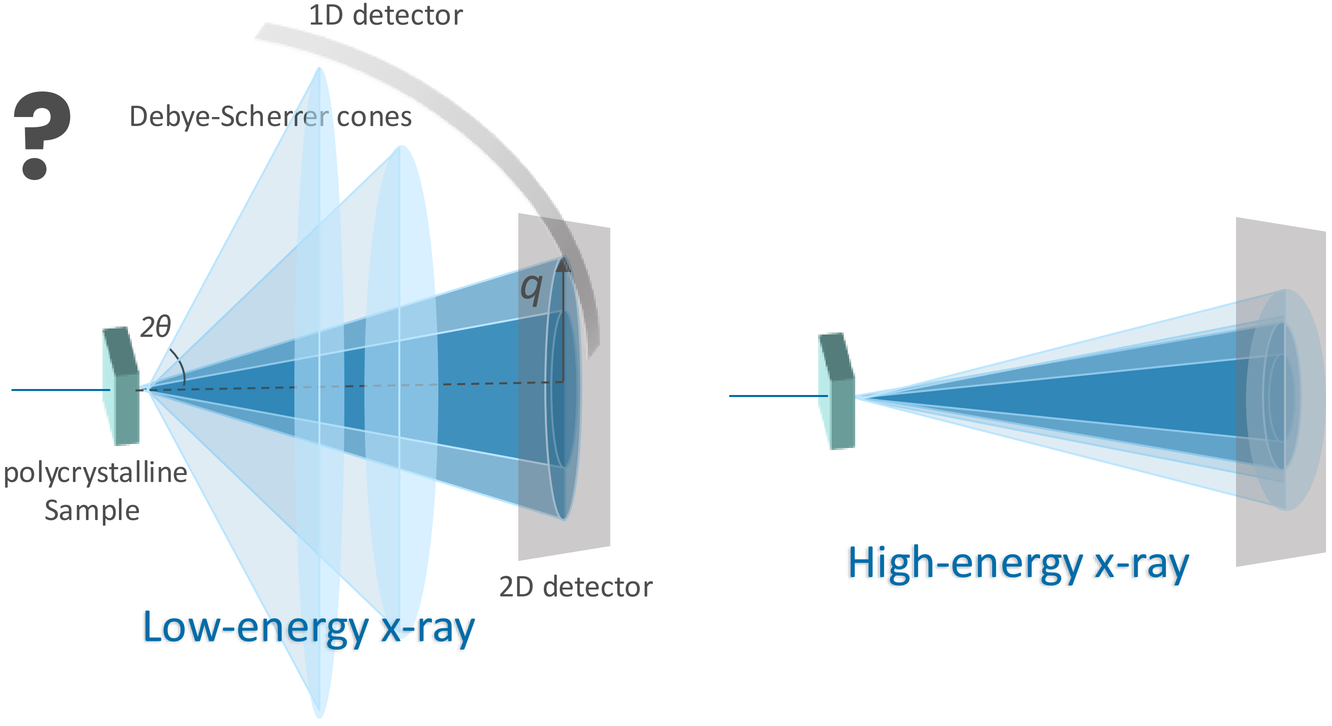

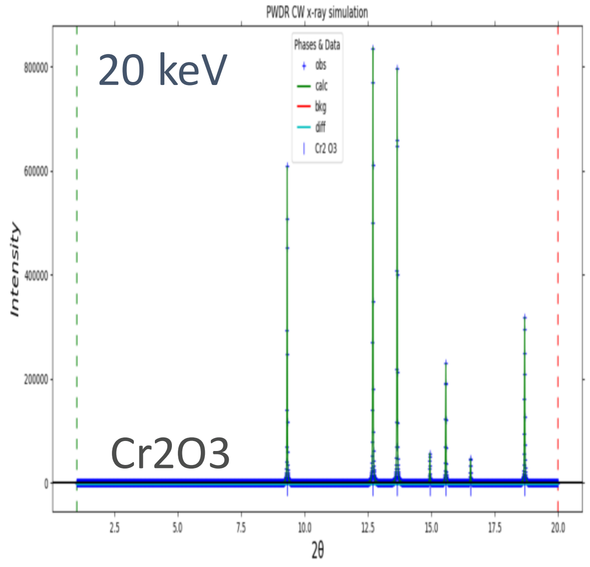

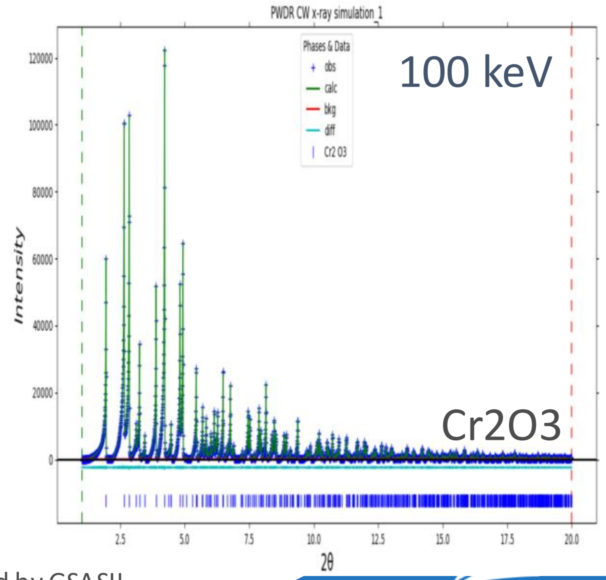

Simulated by GSASII

Capabilities

- ✓ Sample with high-Z elements
- ✓ Thick and large samples, e.g., minerals, large metal pieces

- ✓ In-situ and operando studies
  - ✓ in a complex sample environment
  - ✓ requiring fast data acquisition

Battery charging /discharging

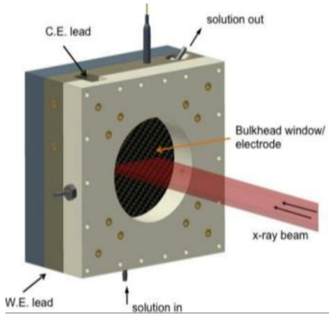

Electrochemical reaction

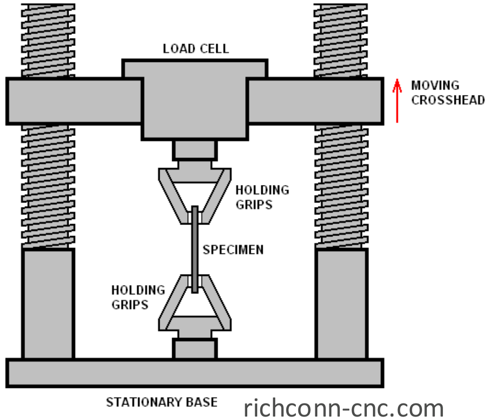

richconn-cnc.com

Mechanical deformation

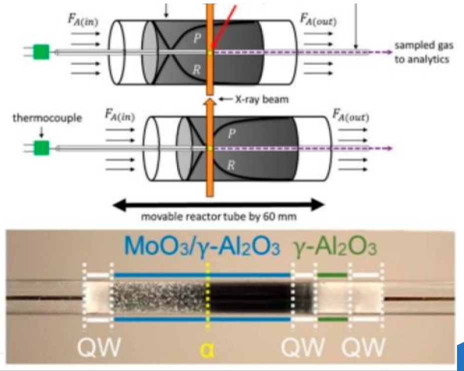

Catalysis studies

Catalysts 2023, 13(11), 1421

ADS 1 & ADS 2 layout

ADS-1

Beam: White or Mono, 50-150 keV
Resolution (ΔE/E): $10^{-2} - 10^{-4}$ (tuneable)
Beam size (FWHM):
Horizontal: max. 17 mm
Vertical: max. 10 mm
min. 80 µm (focusing)

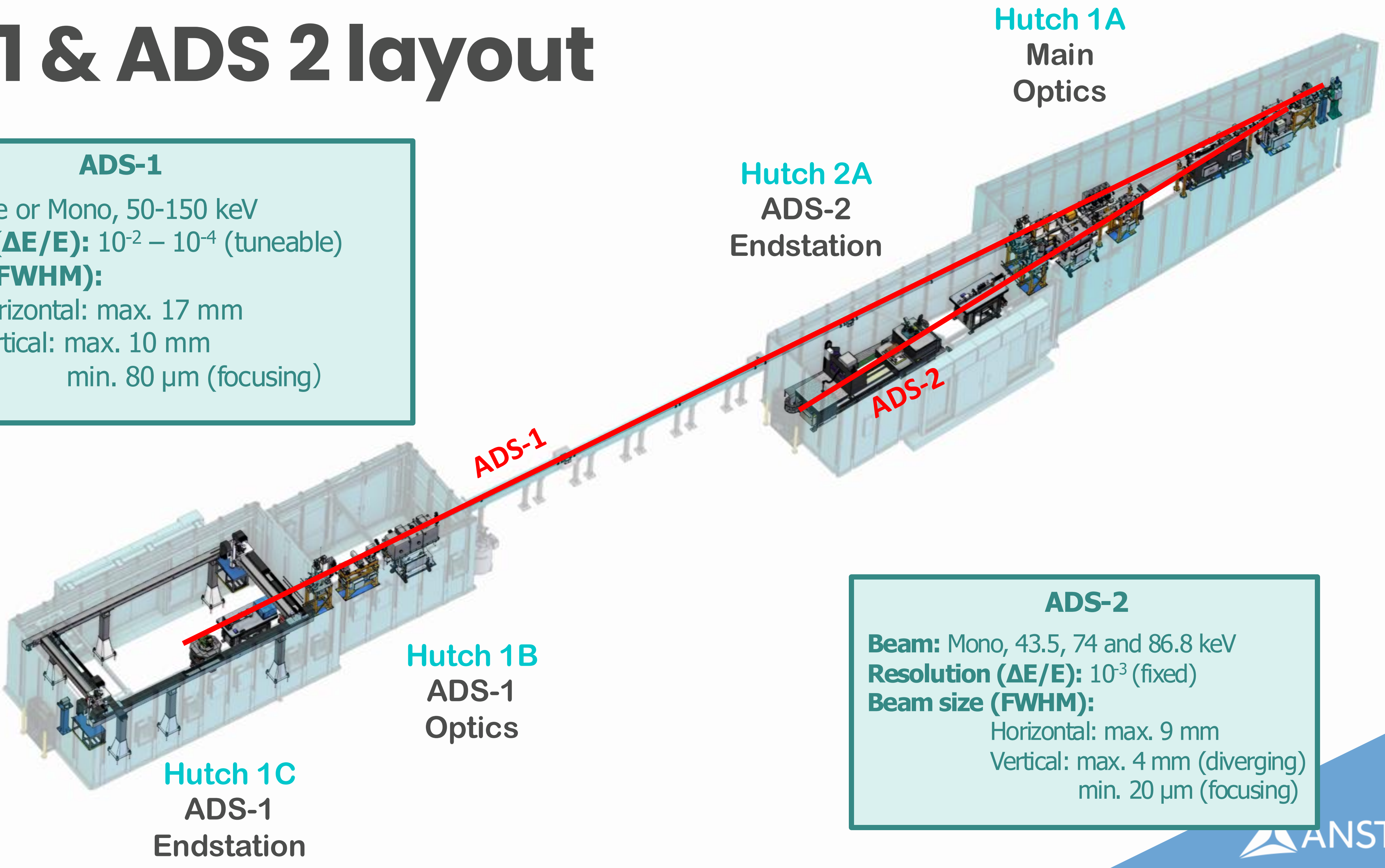

ADS-2

Beam: Mono, 43.5, 74 and 86.8 keV
Resolution (ΔE/E): 10^{-3} (fixed)
Beam size (FWHM):
Horizontal: max. 9 mm
Vertical: max. 4 mm (diverging)
min. 20 µm (focusing)

ANSTO

Some real photos

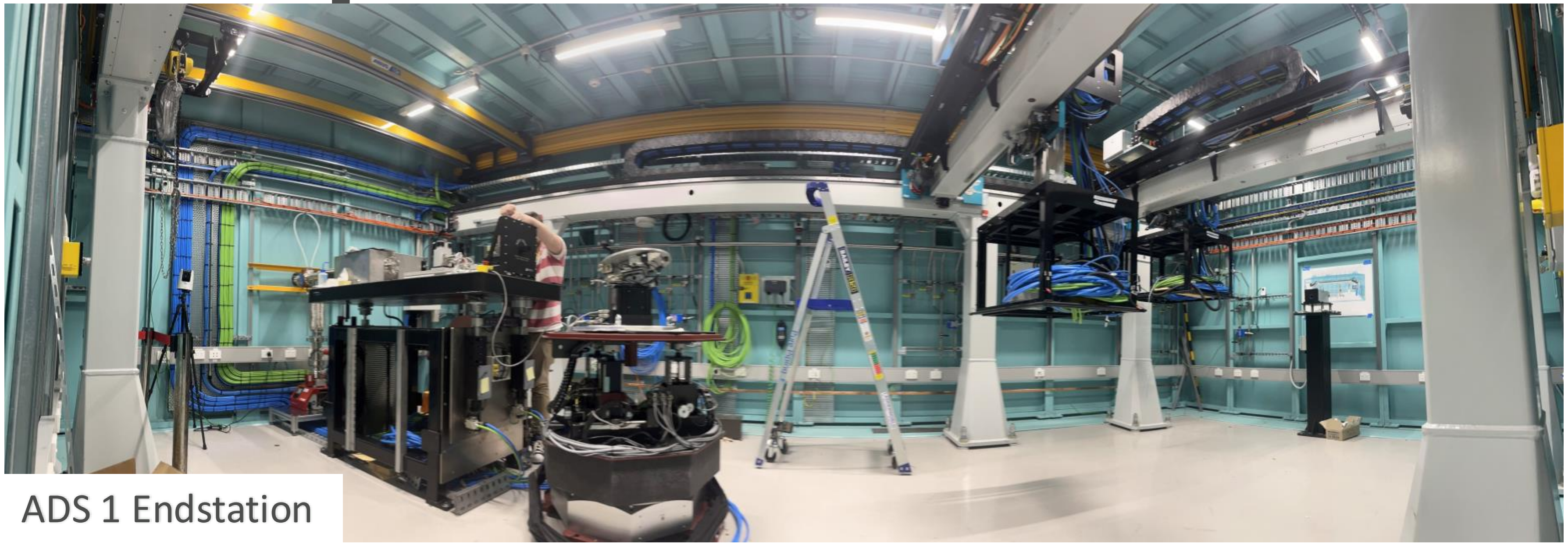

ADS 1 Endstation

User cabin

ANSTO

Sample environment

- T controller
  - Hot air blower (up to 1273 K)
  - Liquid N_2 cryostream (80–400 K)
- Gas environment
  - Various gas supply (H_2, hydrocarbon, CO, CO_2, He, N_2, Ar, O_2 and their mixtures)
  - Supply pressure: 1-60 bar
  - Mass flow controller
  - Gas analyser

More comes later

- Battery charge/discharge sample holder
- Mechanical loading cells
- ? ...Tell us what you'd like!

Or bring your own (contact beamline scientists)

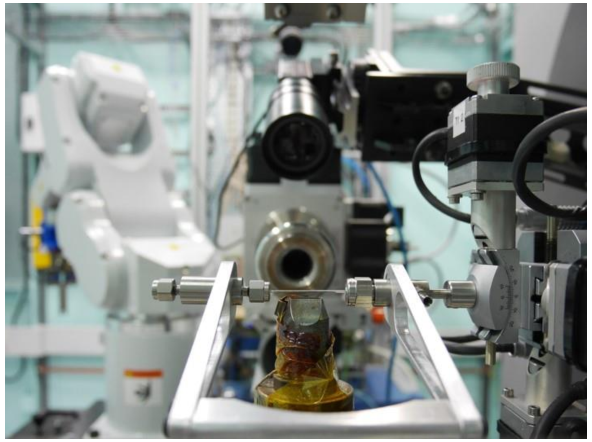

ANSTO

Detectors

- **ADS-1 primary detector:** Eiger2 XE CdTe 9M
  - Hybrid pixel detector – ADS-1 mono diffraction “workhorse”
  - 75 µm pixel pitch
  - max. 550 fps

- **ADS-2 primary detector:** Pilatus3 CdTe 2M
  - 172 µm resolution
  - 250 fps

- **Auxiliary area detector:** Spectrum Logic 3131HS
  - Robust CMOS medical flat-panel detector – far field; white beam
  - 31 x 31 cm active area

- **Imaging detector:** Optique Peter microscope + PCO.edge 5.5
  - 5 MP camera
  - 1X, 2X, 5X selectable objectives
  - ~5–22 mm diagonal FOV

- **Energy-dispersive detector:** Brookhaven custom build (new to synchrotron)
  - 192-element linear array (250 µm pitch)
  - ~1 keV energy resolution

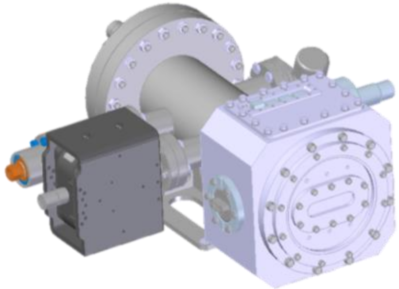

ANSTO

Techniques we offer

- Powder diffraction
- Single crystal diffraction
- Pair distribution function (PDF)
- Energy dispersive diffraction
- Combined diffraction with Imaging and tomography
  - XRD-CT
  - 3DXRD &DCT

ANSTO

Pair distribution function (PDF)

- What it is ?
  - Weighted histogram showing the **distribution of inter-atomic distances**
  - consider both the Bragg's scattering and diffuse scattering
  - Require high q-range to get high resolution
  - Reflect the **short-range disordering** of the materials

- Application
  - Intrinsically Disordered Materials: (amorphous, poorly crystalline, nano-crystalline, or nano-structured materials)
  - Glasses
  - Polymers
  - Pharmaceutical Ingredients

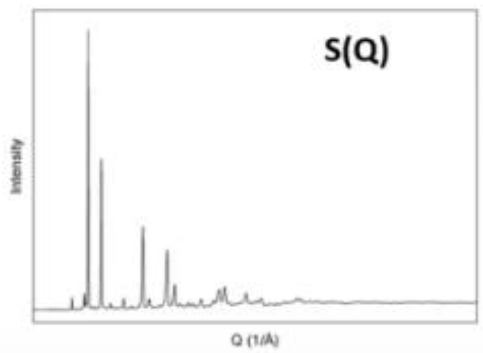

Fourier transformation

$$G(r) = \frac{2}{\pi}\int_0^{\infty} Q[S(Q)-1]\sin(Qr)\,dQ$$

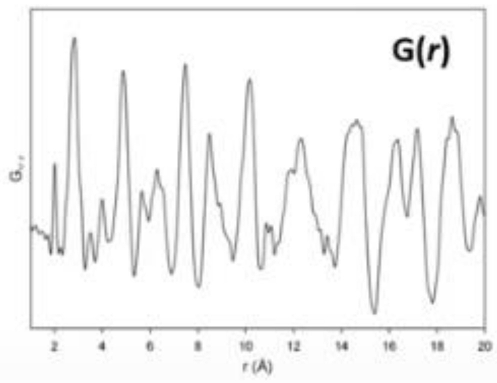

Powder diffraction data

Pair distribution function

Energy dispersive diffraction

Angle-dispersive ("traditional" diffraction): Single wavelength, many diffraction angles

$$n\lambda = 2d\sin\theta$$

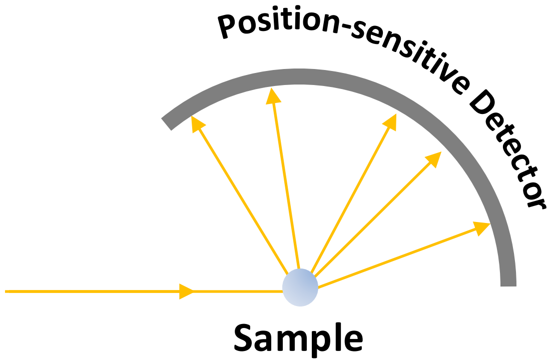

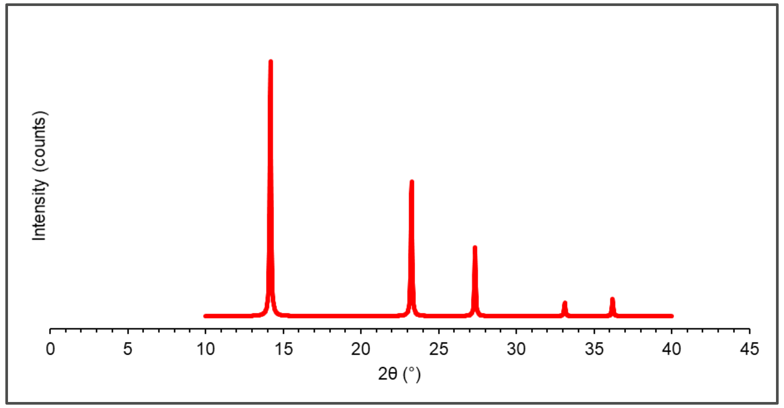

Energy-dispersive: Many wavelengths, one diffraction angle

- Sampled volume ("gauge volume") can be specified
- Can do tomography

$$n\lambda = 2d\sin\theta$$

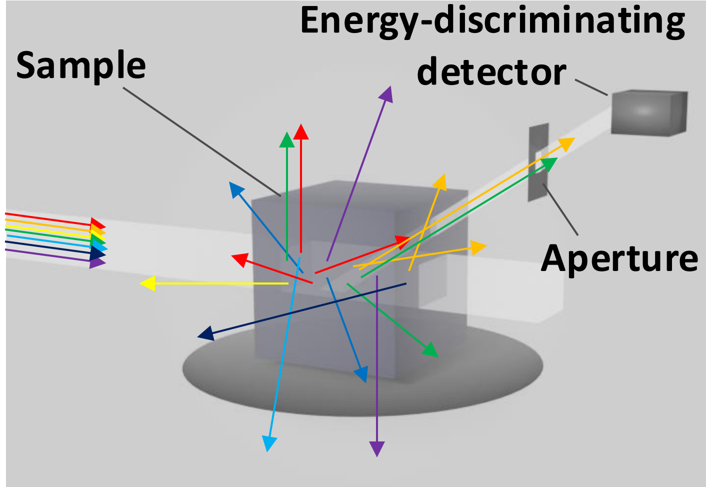

Image: Renata Lippi

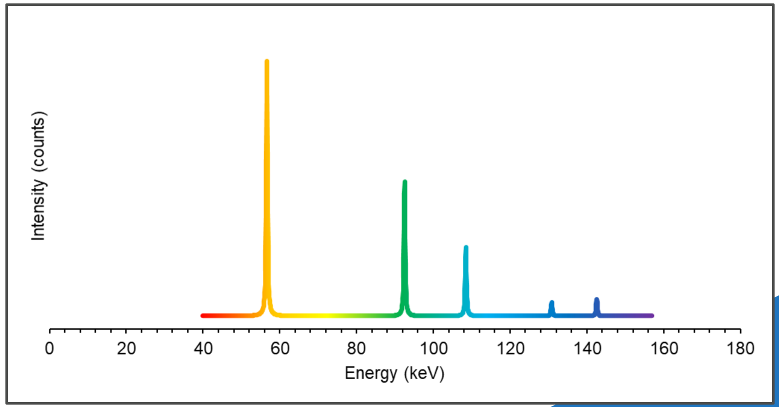

ANSTO

Combined diffraction with tomography

- PXRD + CT data acquisition approach
- 3D maps of the crystalline structure, lattice parameter, crystalline size

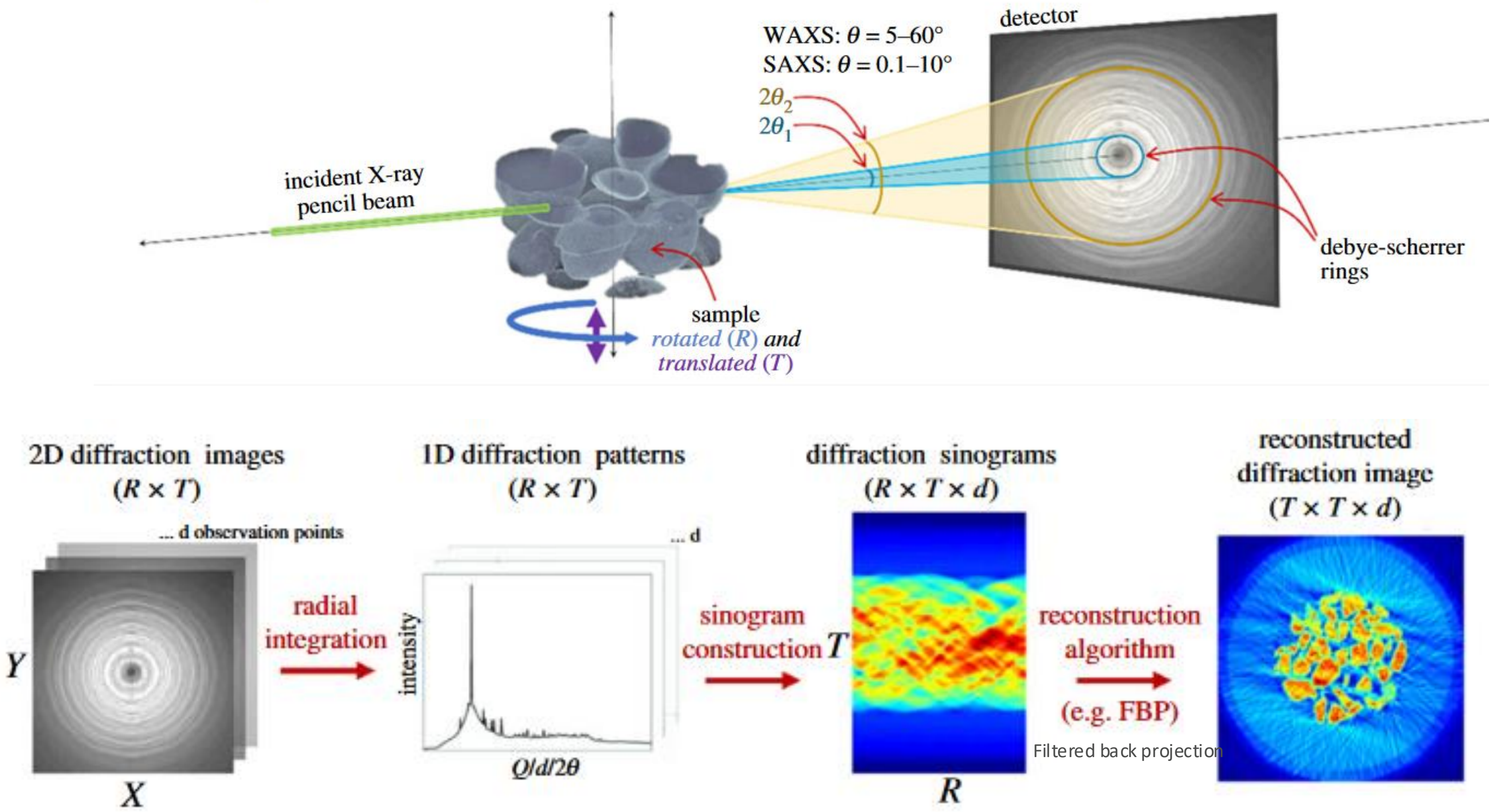

Omori, Naomi E., Antonia D. Bobitan, Antonis Vamvakeros, Andrew M. Beale, and Simon D. M. Jacques. "Recent Developments in X-Ray Diffraction/Scattering Computed Tomography for Materials Science." *Philosophical Transactions. Series A, Mathematical, Physical, and Engineering Sciences* 381, no. 2259 (n.d.): 20220350. https://doi.org/10.1098/rsta.2022.0350.

Combined diffraction and tomography

	Beam focus	Data reconstruction approach	What we obtained	Case studies
XRD-CT	Focused or collimated beam	Using a full 1D powder diffraction pattern for reconstruction	3D maps of crystalline phase	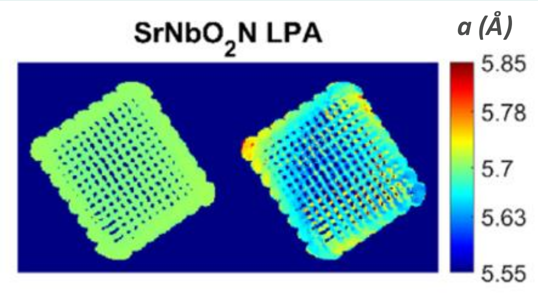 *Materials Advances* 4, no. 16 (August 14, 2023): 3461–72
3D XRD	Highly focused beam	Using isolated diffraction peaks to reconstruct grain maps	Grain orientation and strains	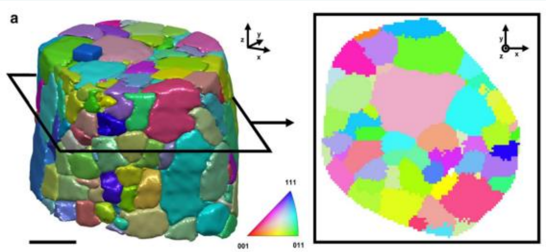 *Acta Materialia 262 (2024) 119419*
DCT (diffraction contrast tomography)	Collimated beam		Intra-grain structures and boundaries	

Science cases from worldwide ADS-like beamlines

In-situ High-energy XRD study of functional fatigue during superelastic load cycling

➢ I12 beamline at Diamond Light Source (DLS, UK)

- Integrating a mechanical loading cell with synchrotron-based high energy X-ray diffraction, the complex interplay between **mechanical loading and microstructural evolution** in Ti-Nb superelastic alloys were studied.

- A two-step degradation mechanism - the role of interfacial defects in driving functional fatigue.
- contributes to the development of fatigue-resistant aerospace materials with enhanced performances and reliability.

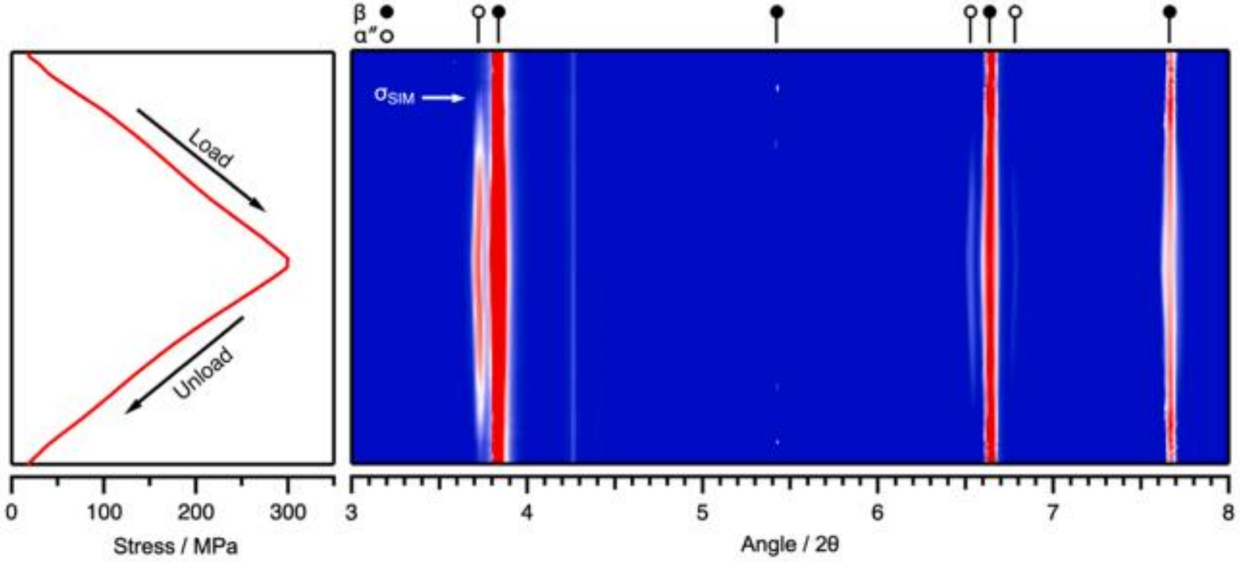

Fig. 6. Intensity map as a function of 2θ angle, during loading and unloading of a sample to 300 MPa.

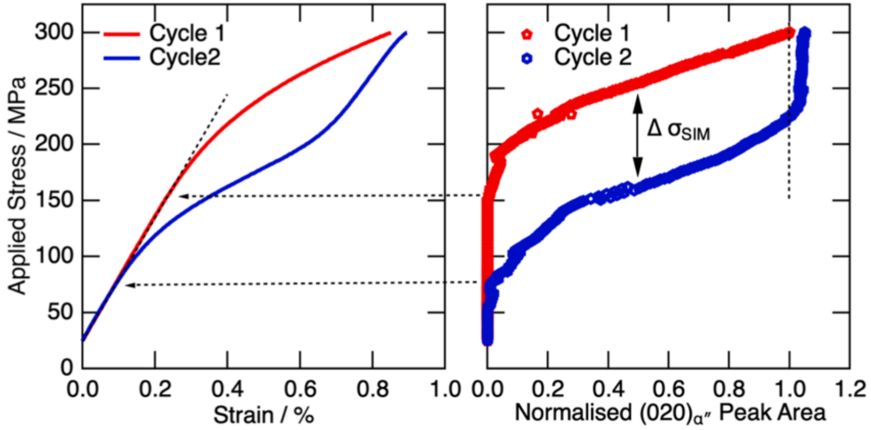

Fig. 8. Left: the loading curves for cycles 1 and 2. Right: Evolution of α″ peak area during loading for cycles 1 and 2, which can be seen to correlate with the deviation from linear elastic behaviour, as shown by the dashed arrows. The peak area achieved in cycle 1 is highlighted by a vertical black dashed line. The peak area in cycles 1 and 2 appear to have a constant offset, consistent with the decrease in σ_{SIM} between these two cycles.

Church, NL, CEP Talbot, LD Connor, S Michalik, and NG Jones. "Functional Fatigue during Superelastic Load Cycling of Ti2448 (Ti-24Nb-4Zr-8Sn, Wt%)." *Materialia* 28 (May 1, 2023): 101719. https://doi.org/10.1016/j.mtla.2023.101719.

In-situ XRD probing the formation kinetics of MOF crystal

➢ I12 Beamline at Diamond Light Source (DLS, UK)

- ✓ **Crystal growth** and **phase formation** of MOF crystal, MFM-300 (Fe) during hydrothermal and solvothermal synthesis

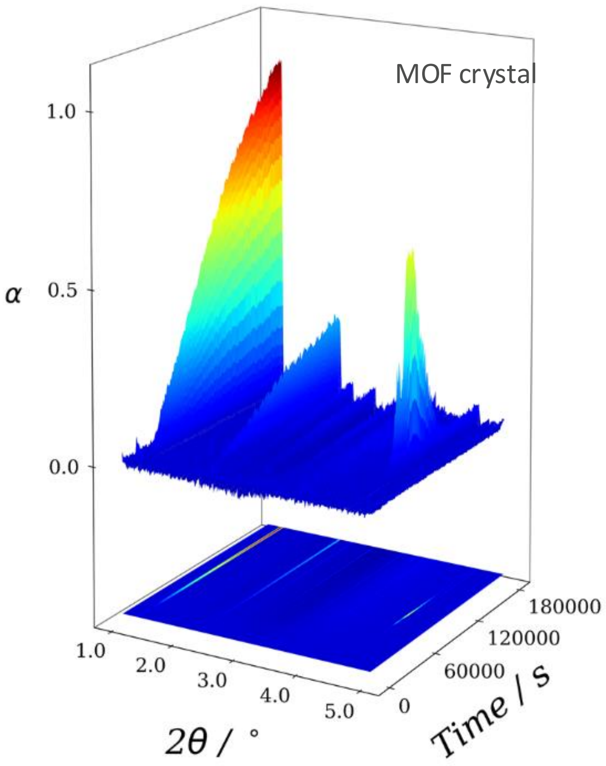

FIG. 3. *In situ* time resolved powder X-ray diffraction patterns of the reaction to form MFM-300(Fe) at concentration **A** at 384.25 K in reaction **I** as a function of extent of crystal growth (α). (Jet color map: blue → red indicates increase in intensity.)

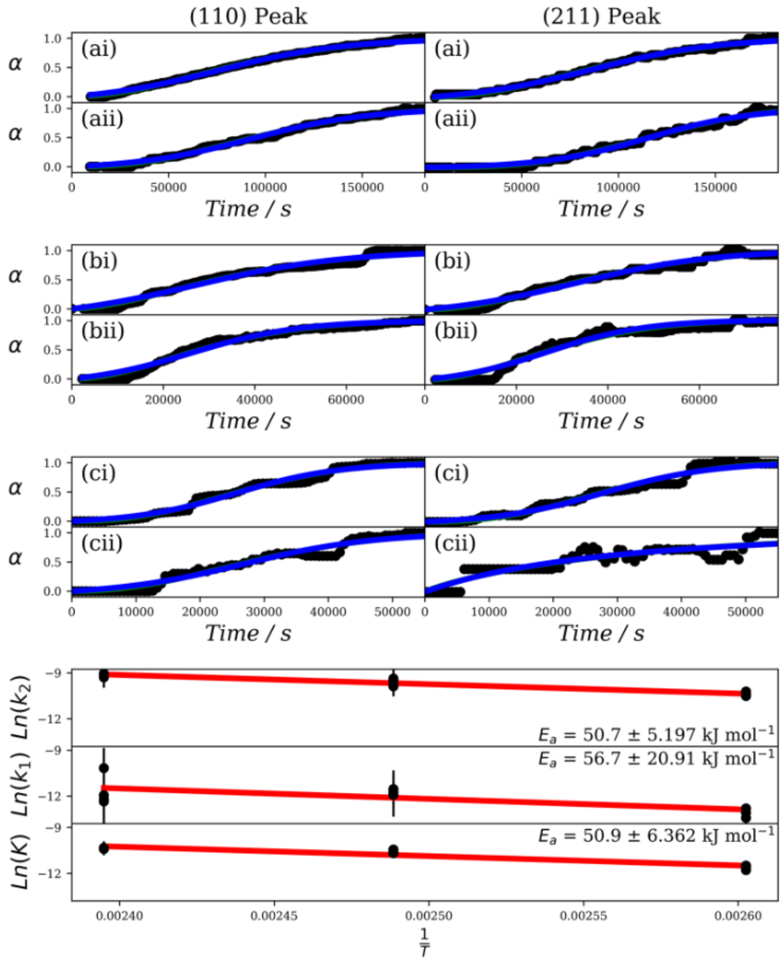

- ✓ **Kinetics** information
  - ✓ Rate constant
  - ✓ Activation energy

Godfrey, Harry G. W., Lydia Briggs, Xue Han, William J. F. Trenholme, Christopher G. Morris, Mathew Savage, Louis Kimberley,et al. "**Analysis by Synchrotron X-Ray Scattering of the Kinetics of Formation of an Fe-Based Metal-Organic Framework with High CO2 Adsorption**." *APL Materials* 7, no. 11 (November 1, 2019): 111104. https://doi.org/10.1063/1.5121644.

ANSTO

Spatially resolved chemical heterogeneities of commercial cylindrical Li-ion batteries by XRD-CT

- P07 at the PETRA III synchrotron at DESY (Hamburg, Germany)
- Operando studies of electrode structures -- mechanisms behind charge storage and degradation.
- **Challenge in accessing internal structural information -** size, thickness, and highly absorbent materials utilized in the casings of commercial cylindrical Li-ion cells (steel)
- High-energy X-rays (~100 keV) serve as an ideal probe

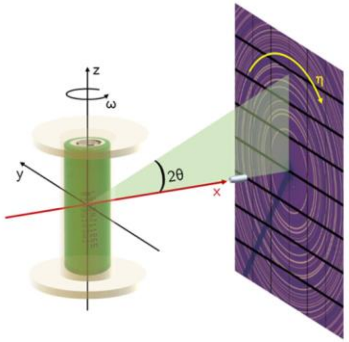

Nature 617, no. 7961 (May 2023): 507–12.

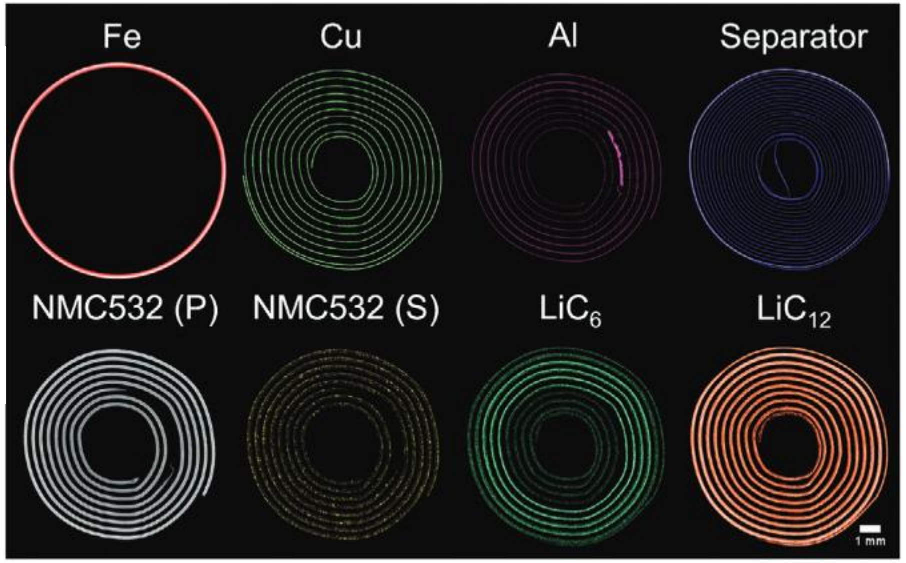

✓ Detailed spatial information of various cell components

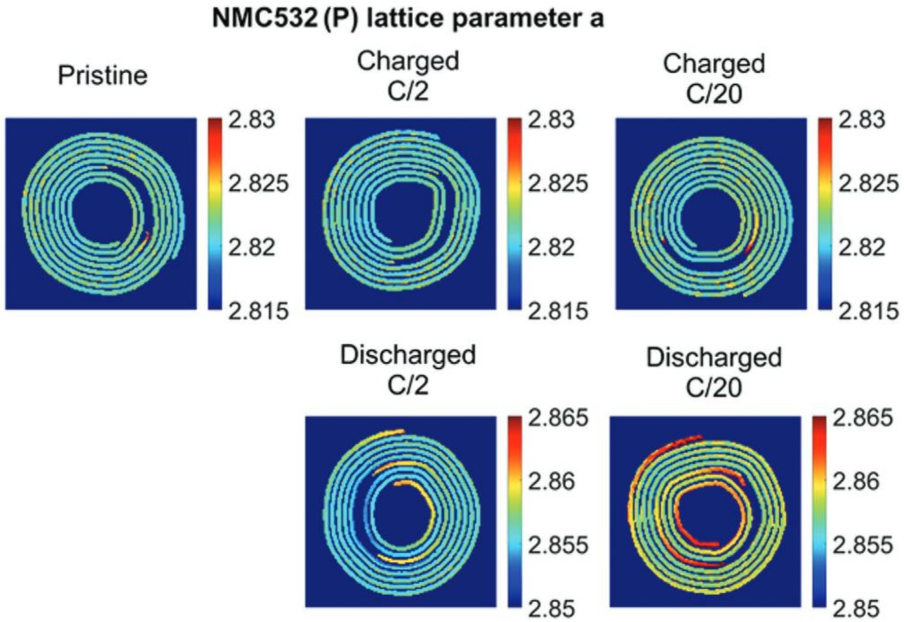

✓ Crystalline phase distribution and lattice parameters -- unravel the presence of inhomogeneous charging and discharging behaviour

Vamvakeros, Antonis, Dorota Matras, Thomas E. Ashton, Alan A. Coelho, Hongyang Dong, Dustin Bauer, Yaroslav Odarchenko, et al. "**Cycling Rate-Induced Spatially-Resolved Heterogeneities in Commercial Cylindrical Li-Ion Batteries**." *Small Methods* 5, no. 9 (2021): 2100512. https://doi.org/10.1002/smtd.202100512.

ANSTO

When we are ready

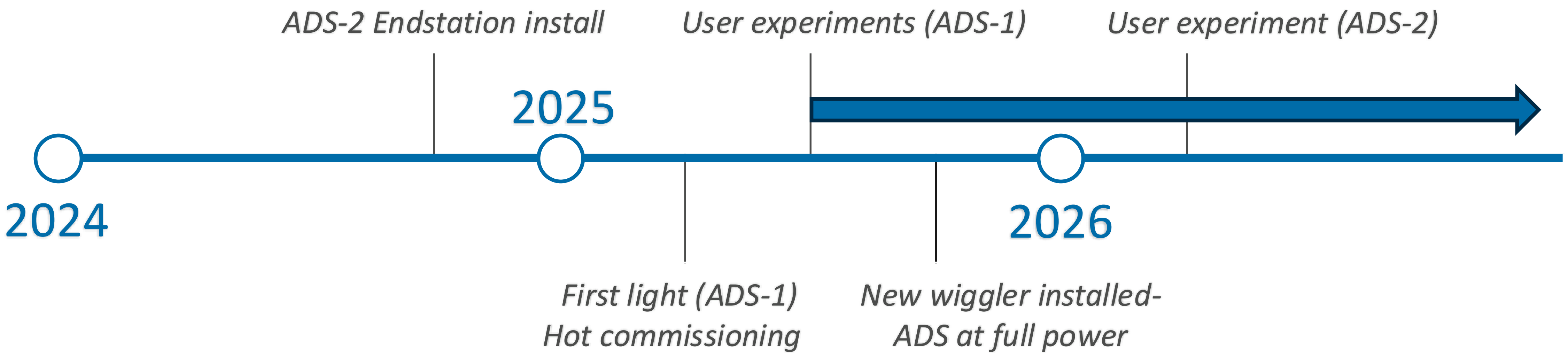

ADS teams

Beamline Team

- Scientists
  - Dr Justin Kimpton (Lead Scientist)
  - Dr Josie Auckett
  - Dr Yang Cao
- Project Manager
  - Gonzalo Conesa-Zamora
- Lead Engineer
  - Sina Porsa
- Controls
  - Brett Alda, Tom Fiala, Ross Hogan,
- PLC
  - Navid Hamedi, Jenna McCoy
- Scientific Computing
  - Emily Massahud Carvalho Ribeiro, Mel Makin, Sinem Ozbilgen, Michelle Chan, Stephen Mudie, Andreas Moll

Technical and Other Support

- Adrian Massey
- Tony Mazonowicz
- Mostafa Haghroosta
- Saber Mostafavian
- Trent Smith
- Brian Jensen
- Rahul Banerjee
- Steve Truban
- Colin Dingfelder
- Jason Wirthensohn
- Nick Sarris
- Nicolas Birkel
- Jonathan McKinlay

Advisory Panel

- A/Prof. John Daniels (UNSW) (Chair)
- Dr Nicholas Armstrong (DSTG)
- Prof. Karena Chapman (Stonybrook)
- Dr Peter Lynch (Deakin)
- Prof. Michael Preuss (Monash)
- A/Prof. Tracy Rushmer (Macquarie)
- A/Prof. Neeraj Sharma (UNSW)

ANSTO

Thank you

as-ads@ansto.gov.au

ANSTO

Time-resolved high-energy X-ray diffraction to understand heat treatment response to supersaturated AM-alloy

➢ I12 Beamline at Diamond Light Source (DLS, UK)

- Additive Manufacturing presents **extremely fast cooling rate** compared to conventional processing methods.
- Recrystallization **occurs within minutes.**
- Time-resolved high-energy XRD (80.291 keV) is conducted to trace the evolution of the γ' volume fraction in Ni-based super alloy with temperature.

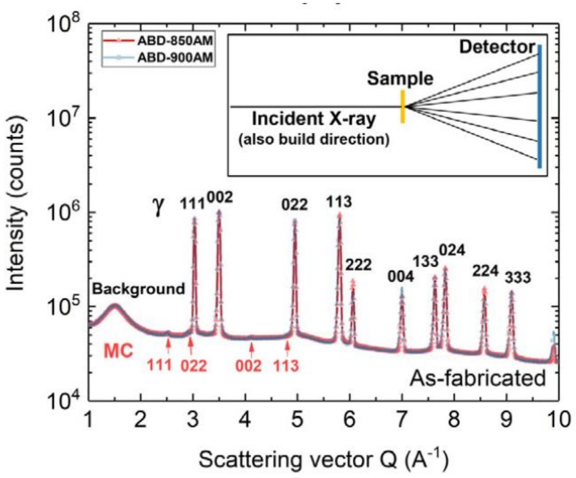

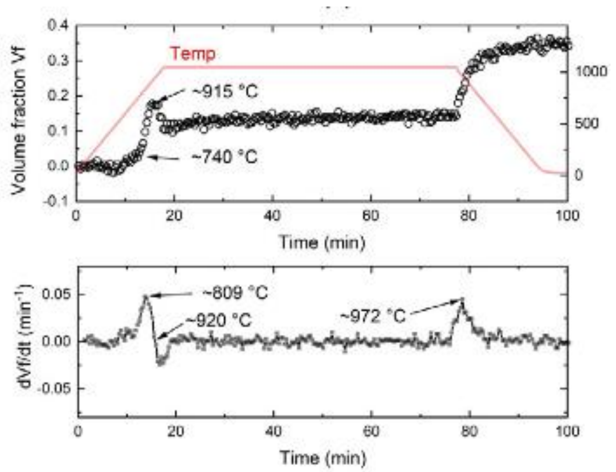

✓ Evolution of γ' precipitate volume fraction during heat treatment

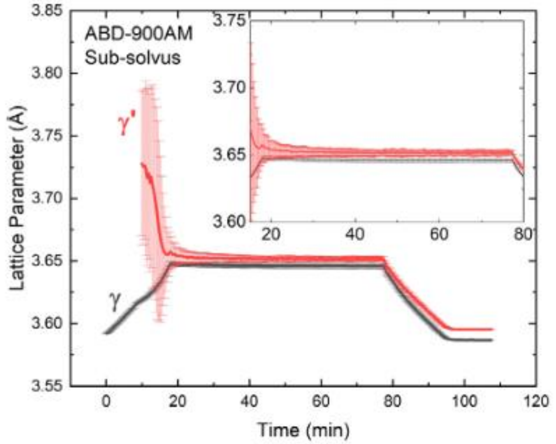

✓ Lattice parameter change as function of heat treatment time

- Insights on a new strategy of tailoring microstructure for additively manufactured superalloys by manipulation of the γ' **precipitate distribution upon heating**.

Tang, Yuanbo T., Chinnapat Panwisawas, Benjamin M. Jenkins, Junliang Liu, Zhao Shen, Enrico Salvati, Yilun Gong, et al. "Multi-Length-Scale Study on the Heat Treatment Response to Supersaturated Nickel-Based Superalloys: Precipitation Reactions and Incipient Recrystallisation." *Additive Manufacturing* 62 (January 25, 2023): 103389. https://doi.org/10.1016/j.addma.2023.103389.

Understand the grain structure of superelastic alloy during intensive plastic deformation

- BM32 beamline at ESRF, B16 test beamline at DLS
- to unveil the evolution of lattice rotation, strain field, and phase transformation at micro- and mesoscale levels, quantifying the impact of grain structure on SE performance

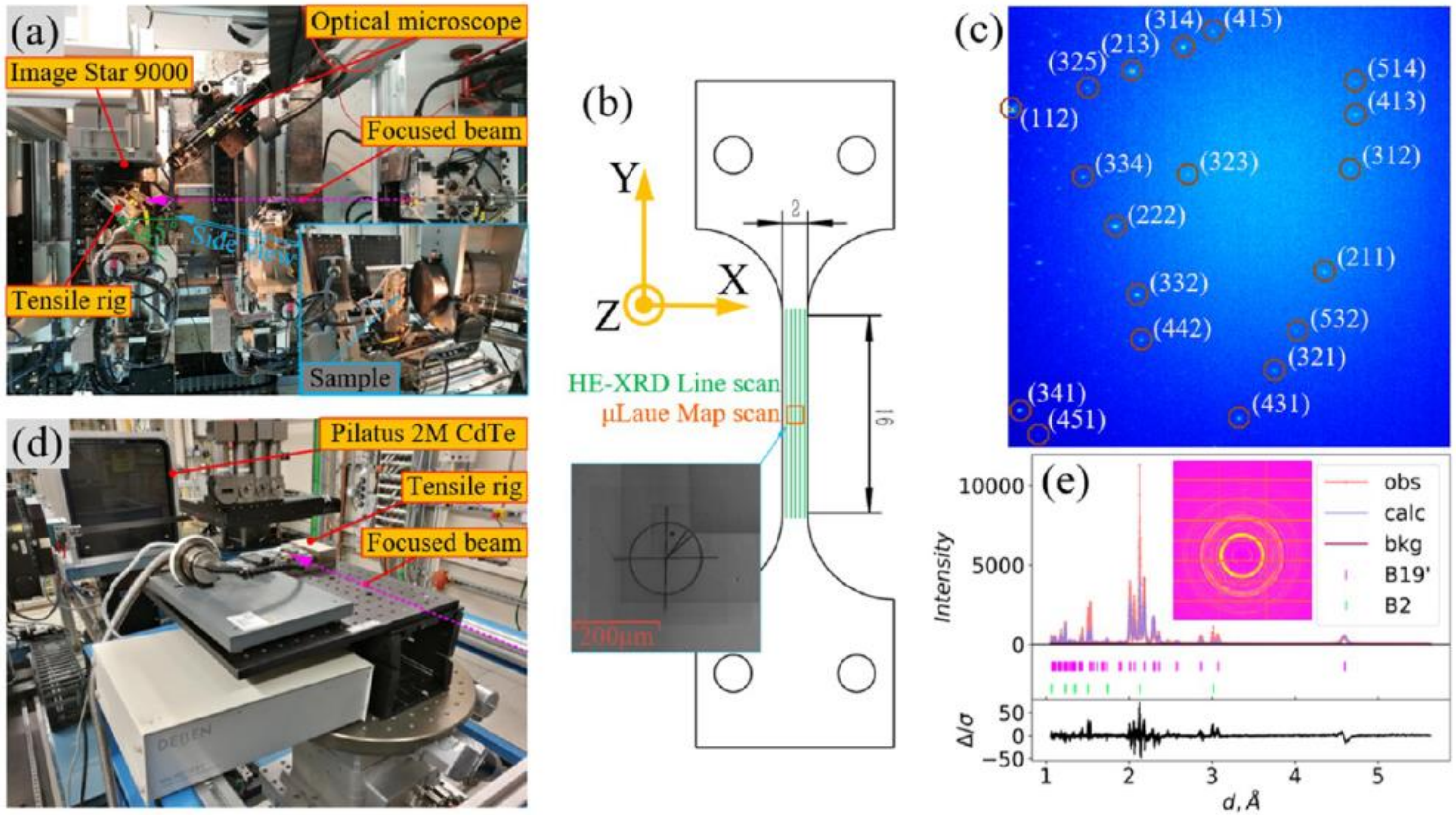

μLaue microdiffraction
- White beam
- Crystal orientation and symmetry

Powder diffraction
- Monochromatic beam
- Phase formation

- Three distinct grain lattice rotation modes have been identified and asymmetric strain distribution has been observed during loading.

Wang, Zifan, Jingwei Chen, Radim Kocich, Samuel Tardif, Igor P. Dolbnya, Lenka Kunčická, Jean-Sébastien Micha, et al. "Grain Structure Engineering of NiTi Shape Memory Alloys by Intensive Plas Deformation." *ACS Applied Materials & Interfaces* 14, no. 27 (July 13, 2022): 31396–410. https://doi.org/10.1021/acsami.2c05939.

ANSTO

Beamline structure